Automated Grasp Point Generation for Wire Grippers in Binder-Jet Metal Additive Manufacturing

Qihan Wang[1], Kenji Shimada[2]
Department of Mechanical Engineering, Carnegie Mellon University

***Abstract*—De-powdering is a critical step in binder jet metal additive manufacturing, which requires efficient and automated solutions to remove residual powder while maintaining part integrity. This research presents a novel algorithm for generating grasp point candidates on any 3D objects using wire grippers wires bent in certain directions. The method involves projecting STL models onto a 2D bitmap to extract a silhouette, applying morphological dilation and contour detection to identify key boundary features, and classifying grasp points based on curvature analysis. A direction-aware selection process determines four optimal grasping points with corresponding orientations, ensuring stable lifting configurations. The grasping strategy is further validated in NVIDIA Isaac Sim through physics-based simulations, where wire grippers attempt to lift and stabilize parts. The results demonstrate the robustness of the proposed approach in identifying reliable grasp points for diverse 3D geometries, paving the way for automated depowdering solutions in industrial additive manufacturing workflows. The progress in the solution establishes binder jet metal 3D printing as a cutting-edge method for producing complex, high-performance parts with diverse industrial applications. This research drives additive manufacturing forward by opening up new opportunities for scalable and flexible production systems in contemporary industry.**

I. Introduction

Powder-bed-based additive manufacturing (PBAM) techniques, such as powder-bed fusion and binder jetting, have been widely studied since the 1980s for manufacturing sophisticated geometries [1]. Depowdering, a crucial step following PBAM processes, involves extracting printed parts from the surrounding powder bed. This process typically includes manual techniques, such as brushing, to remove loose powder. Significant research has been conducted on automating the removal of unbound powder, utilizing robotic arms and specialized de-powdering stations to enhance efficiency and mitigate operator health risks.

Removing external powder from printed parts is generally straightforward. Traditional techniques include manual brushing, air blowing, and vibration-assisted powder removal [2]. Although these methods can be effective for certain geometries, they often struggle with complex internal channels and delicate structures, risking damage to parts and leaving residual powder in areas difficult to reach [3]. Advanced systems, such as Solukon's Smart Powder Recuperation (SPR) technology, utilize programmable rotation and vibration to remove powder from intricate geometries.

Following the depowdering phase in the manufacturing of binder jetting additives, the subsequent challenge involves securely grasping and transferring delicate parts from the powder bed to storage or processing areas without causing damage. One notable grasping approach is the use of the finger gripper. The Generative Grasping Convolutional Neural Network (GG-CNN), which predicts grasp quality and pose directly from depth images, enables real-time grasping with a three-finger gripper [4]. Typically, multiple identical and fragile printed parts are arranged in a three-dimensional grid within a box filled with metal powder. Applying force directly to these parts using a traditional finger gripper can risk damaging their delicate structures, which is critical to avoid in preparation for subsequent processing steps. In addition, grasping a single part with a finger gripper can disturb the surrounding parts, causing positional deviations within the powder bed. To overcome these challenges, novel automated grasping methods have been developed to enable gentle and precise part extraction without compromising the integrity of adjacent components.

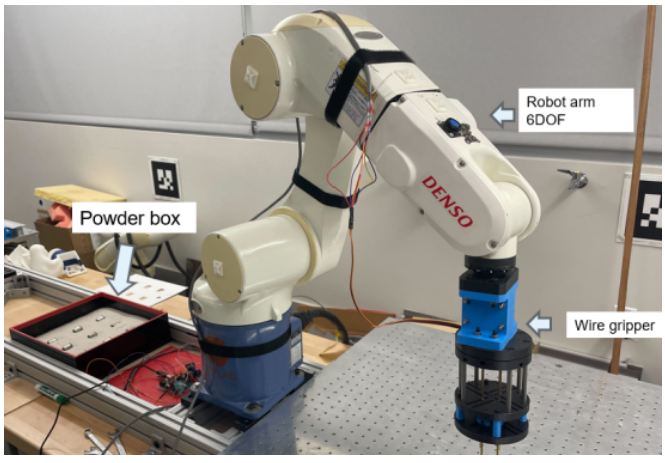

Fig. 1. Overview of the Workstation Setup, Featuring the Denso VS6577 B 6DOF Robot Arm, Intel RealSense L515 Camera, and Novel Wire Gripper.

In the context of automation, wire grippers have gained significant attention for handling parts within metal powder beds. Compared to traditional finger grippers, wire grippers

have a flexible and slender design, allowing them to navigate through confined spaces without disturbing adjacent parts [5]. The wires with specially bent ends gently embrace the components below, providing secure handling without applying damaging pressure. This makes wire grippers particularly suitable for grasping delicate or intricate components safely and efficiently during the critical depowdering process. There are multiple benefits that our wire gripper system could offer:

- Enabling fully automatic, labor-free de-powdering and part extraction processes to enhance production efficiency.
- Using wire grippers to gently embrace parts from the bottom, minimizing the risk of damaging fragile structures.
- Preventing displacement of neighboring parts during extraction by allowing precise, localized grasping without external disturbance.
- Offering a simple, low-cost, and easily repairable solution compared to complex robotic handling systems.

In this work, we introduce a novel algorithm designed specifically to identify optimal grasp points on 3D objects for wire grippers. The proposed method involves projecting STL models onto 2D bitmaps to extract silhouettes, applying morphological dilation, and conducting curvature analysis to classify and select suitable grasping points and orientations. By generating stable and efficient lifting configurations, this approach significantly advances automated depowdering solutions in metal additive manufacturing workflows. The effectiveness of the identified grasping positions and orientations will be validated through physics-based simulations using NVIDIA Isaac Sim, ensuring robust and reliable grasping performance in practical scenarios.

II. Related Works

Removing powder from additively manufactured components presents a significant technical challenge due to their delicate nature. A key requirement is operational flexibility, as conventional finger and jaw grippers struggle to conform to varied AM part geometries, resulting in inadequate grip and potential damage during depowdering.

Researchers have explored various gripper designs for handling sensitive additive manufacturing parts. Compliant grippers have been developed to automate the extraction of 3D printed parts from unfused PA12 powder, improving handling through flexible mechanics [6]. Bioinspired soft robotic grippers have also been introduced, capable of adapting to complex geometries while minimizing damage through gentle control, with electrostatic adhesion further enhancing adaptability for fragile objects [7]. Adjustable robotic grippers have been shown to reduce risk of deformation, outperforming traditional tools in handling various shapes of objects [8]. In addition, studies on binder jetting processes have examined methods to mitigate part deformation, although these focus primarily on powder behavior rather than post-processing challenges [9].

Unlike traditional finger and jaw grippers that depend on convolutional neural networks (CNN) trained on synthetic

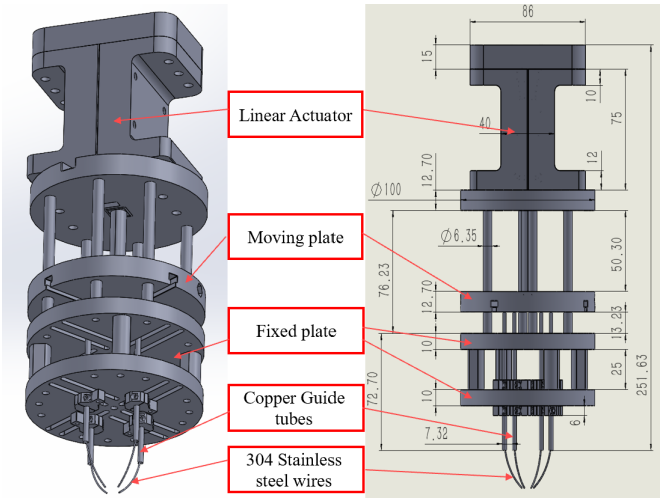

Fig. 2. Design schematic for the noval wire gripper

object grasp datasets, such as MVGrasp, which generates pixel-wise grasp synthesis maps indicating grasp quality, orientation, and gripper width [10], the wire gripper developed in this study is specifically engineered for reliable handling of closely positioned parts. Constructed from deformable 304 stainless steel wires, the gripper gently embraces objects from below, thereby minimizing friction and eliminating the need for lateral forces or pressure. This approach is particularly advantageous for dense additive manufacturing trays, as it significantly reduces the risk of damaging fragile components and prevents disturbance of neighboring parts during extraction.

Significant effort has been put into the development of the adaptive wire gripper in our group. The system functions as a precise and compliant holder designed to maintain the structural integrity of delicate small green components. A linear actuator governs the synchronized vertical movement (Z-axis) of all the attached wires with diameter $0.8mm$. During operation, the actuator extends, causing the deformable wires to protrude from the $1/8''$ internal diameter copper guide tubes and gently enclose the target part from underneath. Upon retraction, the wires are withdrawn into the tubes, allowing the part to be released into the designated storage area. Furthermore, the modular design incorporates adjustable slots that enable repositioning of the wires and copper tubes, thereby accommodating a wide range of part sizes and complex geometries. The arrangement of multiple wires, attached to flexible cables, enables the gripper to adapt to the surfaces of the parts and apply a uniform gripping force, thus mitigating the risk of mechanical damage during handling.

III. Methodology

The proposed grasp planning and validation framework is composed of two main modules: a grasp pose analysis module and a physical simulation validation module, operating sequentially to ensure robust wire gripper deployment. In the first stage, the grasp pose analysis module processes

a 3D object mesh by projecting it onto the XY-plane to generate a binary offset silhouette representation. Contour extraction, morphological operations, and curvature analysis are then applied to identify candidate grasping points along the boundary of the object. Valid quadruples of grasp points are selected based on their ability to enclose the object centroid and meet stability criteria and geometric constraints, resulting in a collection of feasible grasp configurations. In the second stage, the physical simulation validation module employs NVIDIA Isaac Sim to assess each grasp combination under realistic physics-based interactions. The wires are instantiated and positioned according to the proposed grasp points, and grasping actions are simulated to evaluate success rates, object stability, and robustness against disturbances.

A. Mesh Preprocessing

The grasp planning pipeline begins with the preprocessing of a 3D object mesh $\mathcal{M}$, represented as a set of vertices $\mathbf{V}$ and triangles $\mathbf{T}$:

$$\mathcal{M} = (\mathbf{V}, \mathbf{T}) \tag{1}$$

The mesh is loaded from an STL file and normalized if necessary. Vertex normals are computed to facilitate downstream tasks. This step ensures consistent scaling and orientation before projection.

B. Bitmap Projection

To simplify the grasp planning process, the 3D mesh is projected onto the XY plane, ignoring the Z-dimension:

$$(X, Y) = (V_x, V_y) \tag{2}$$

The projected vertices are scaled and centered within a bitmap of size (W, H) using the following transformations:

$$X' = (X - x_c) \times s + \frac{W}{2} \tag{3}$$

$$Y' = H - \left((Y - y_c) \times s + \frac{H}{2} \right) \tag{4}$$

where s is a scaling factor and (x_c, y_c) is the centroid of the projected vertices. Triangular faces are rasterized to produce a binary silhouette image $\mathcal{I}$.

C. Contour Extraction and Point Sampling

The generation of grasp candidates begins with the extraction of expanded contours from the binary image $\mathcal{I}$. This binary representation facilitates the identification of transitional boundaries between black and white regions in the grayscale image, effectively defining the object's contour.

Contour expansion is a critical consideration in this methodology, as feasible grasp points cannot be positioned directly on the object's edge. An appropriate offset must be maintained to account for both the physical diameter of the wire gripper and the necessary clearance between the wire and the object's surface. To achieve this offset, we implement an iterative dilation process in which each iteration expands the contour by one pixel. For the experiments described here, the number of dilation iterations was empirically determined to be 150.

To optimize computational efficiency while maintaining representative sampling, we introduce a target point count parameter. This approach enables systematic downsampling of contour points through uniform reduction, which precisely yields $n_{\text{target}} + 1$ points along the expanded contour. The resulting sample points provide a balanced representation of the object's geometry without excessive computational overhead.

Algorithm 1: Contour Expansion and Point Sampling

Input: Binary bitmap $\mathcal{I}$, target number of points n_{target}

Initialize the desired number of dilation iterations n_{iter};
while *True* **do**
  Reset binary bitmap $\mathcal{I}_b \leftarrow (\mathcal{I} < 128)$;
  for $i \leftarrow 1$ **to** n_{iter} **do**
    Apply morphological dilation to $\mathcal{I}_b$;
  Extract contours $\mathcal{C}$ from $\mathcal{I}_b$;
  Initialize $total\_points \leftarrow 0$, $converted\_points \leftarrow \emptyset$;
  for *each contour* c *in* $\mathcal{C}$ **do**
    $r \leftarrow \max(1, \text{len}(c)/n_{\text{target}})$;
    Subsample contour $c_{\text{sampled}} \leftarrow c[:: r]$;
    for *each point* (X', Y') *in* $c_{sampled}$ **do**
      if $0 \leq x < W$ ***and*** $0 \leq y < H$ **then**
        Transform (X', Y') back to real-world scale;
        Append transformed point to $converted\_points$;
        $total\_points \leftarrow total\_points + 1$;
  if $total\_points = n_{target} + 1$ **then**
    break;
  else
    $n_{\text{iter}} \leftarrow n_{\text{iter}} + 1$;
return $converted\_points$;

Following contour extraction and sampling, the bitmap coordinates must be transformed back to the real-world coordinate system. This transformation is accomplished through the following equations:

$$x_{convert} = \frac{x - \frac{W}{2}}{s} + x_c \tag{5}$$

$$y_{convert} = \frac{H - y - \frac{H}{2}}{s} + y_c \tag{6}$$

Contours $\mathcal{C}$ are extracted and sampled uniformly to generate a set of candidate points:

$$\mathcal{P} = \{p_i\}_{i=1}^{N} \subset \mathcal{C} \tag{7}$$

This process ensures an even distribution of points along the object's silhouette.

D. Curvature Analysis

In the context of wire gripper grasping, it is particularly important to avoid selecting grasp points located at convex corners. Grasping at sharp convex edges can cause mechanical instability, as any disturbance or vibration during the grasping process may cause the wire to slip off the edge, resulting in grasp failure. To mitigate this risk, points exhibiting strong convexity, identified by large negative curvature angles, are excluded from the set of valid grasp candidates.

Each sampled point p_i along the object contour is analyzed to estimate the local curvature, which is crucial for ensuring stable grasping. To compute the curvature at a point p_i, two neighboring vectors are considered: v_1 connecting p_{i-1} to p_i, and v_2 connecting p_i to p_{i+1}:

$$\delta\theta_i = \text{atan2}(v_{2y}, v_{2x}) - \text{atan2}(v_{1y}, v_{1x}) \tag{8}$$

$$\delta\theta = [(\delta\theta_i + \pi) \bmod (2\pi)] - \pi \tag{9}$$

The equation computes the minimal signed angle difference between two vectors $\mathbf{v}_1$ and $\mathbf{v}_2$ using their atan2 angles. By first normalizing the raw angular difference into $[0, 2\pi)$ via $\bmod$ and then shifting to $[-\pi, \pi)$, it ensures the result represents the shortest rotational path between vectors, with sign indicating direction (positive for counterclockwise, negative for clockwise). This is particularly useful for orientation calculations in robotics and motion planning.

Based on the angle $\delta\theta_i$, points are classified as:

- **Concave** if $\delta\theta_i > 10^\circ$.
- **Convex** if $\delta\theta_i < -10^\circ$.
- **Flat** otherwise.

Adjacent points of convex points are also promoted as convex to enhance grasp stability. Classification facilitates efficient generation of grasp candidates.

E. Grasp Candidate Selection

Vectors $\mathbf{d}_i$ between neighboring contour points are computed to estimate the local surface tangent direction at each point. Specifically, for a given point p_i, the vector $\mathbf{d}_i$ is defined as the difference between the coordinates of its adjacent points p_{i+1} and p_{i-1}. The grasp approach direction $\mathbf{n}_i$ is then determined by rotating $\mathbf{d}_i$ counterclockwise by 90°.

This ensures that the grasping direction is always orthogonal to the local surface tangent, pointing inward relative to the object's contour. Such a configuration is crucial for minimizing slippage and maximizing contact stability during the lifting motion.

Quadruples of grasp points are generated by selecting non-convex (i.e., concave or flat) points at regular intervals along the contour. The selection ensures spatial distribution and mechanical stability. A quadruple of grasp points is considered valid only if it satisfies the following two conditions:

1) The grasp polygon must enclose the object's center (x_c, y_c).
2) The centroid of the grasp polygon must be within a specified distance $d_{\max}$ from (x_c, y_c).

This ensures grasp stability and symmetry around the object's center of mass.

Algorithm 2: Selection of Valid Grasping Quadruples

Input: Set of candidate points $\mathcal{P}$, object centroid (x_c, y_c)

```
Set numofinterval ← n;
Compute distance_threshold based on object bounding box dimensions;
Initialize valid_combinations ← ∅;
for each 4-tuple combo generated from {0, 1, ..., m − 3 × n} do
    Adjust selected positions using interval spacing;
    if all selected positions are valid then
        Construct polygon poly from selected points;
        if poly contains (x_c, y_c) then
            Compute centroid (x_cp, y_cp) of poly;
            Calculate distance d;
            if d ≤ distance_threshold then
                Append to valid_combinations;
return valid_combinations;
```

F. Hook Placement and Pose Estimation

Once valid combinations for grasp quadruples are identified, hooks are placed at the selected points. Each grasp point $p_i = (x_i, y_i)$ with an associated orientation θ_i is transformed using a homogeneous transform:

$$R(\theta)_z = \begin{bmatrix} \cos(\theta_i) & -\sin(\theta_i) & 0 & x_i + x_c \\ \sin(\theta_i) & \cos(\theta_i) & 0 & y_i + y_c \\ 0 & 0 & 1 & z \\ 0 & 0 & 0 & 1 \end{bmatrix} \tag{10}$$

where $R(\theta_i)$ is the 2D rotation matrix and t_i is the translation vector. Hooks are instantiated, transformed, and merged with the original object mesh to visualize feasible grasp configurations.

G. Validation of Grasping Success in Physics Simulation

The efficacy of grasping mechanisms was rigorously validated through computational simulation utilizing the NVIDIA Isaac Sim environment, which implements accurate physical dynamics. The experimental apparatus comprised a central target object and four strategically located articulated hooks affixed to stationary bases. The spatial configuration of these components was precisely defined using quaternion transformations to establish proper orientations. Since there is no rotation on the x-axis and the y-axis: $\theta = 0$, $\phi = 0$. The quaternion q_{1B} representing a rotation of angle ψ around the x-axis is given by the following.

$$q_z = \begin{bmatrix} (1)(1)\cos(\psi/2) + (0)(0)\sin(\psi/2) \\ (0)(1)\cos(\psi/2) - (1)(0)\sin(\psi/2) \\ (1)(0)\cos(\psi/2) + (0)(1)\sin(\psi/2) \\ (1)(1)\sin(\psi/2) - (0)(0)\cos(\psi/2) \end{bmatrix} = \begin{bmatrix} \cos(\psi/2) \\ 0 \\ 0 \\ \sin(\psi/2) \end{bmatrix} \tag{11}$$

This quaternion representation facilitates the accurate modeling of rotations in a three-dimensional space. The prismatic joints connecting the bases to their respective hooks were parameterized with large stiffness and damping coefficients and were restricted to traverse exclusively along the z axis.

To determine the successful grasping sets, the algorithm needs to track the object's position and orientation during the lifting process to detect if it falls or tilts excessively.

- **Object falling** Tracks the vertical position of the object and detects if it falls below a certain threshold compared to the position of wires at every time step.
- **Object tilting** Monitors the orientation of the object throughout the simulation and calculates the angular deviation from its initial orientation. If the tilt exceeds a predefined threshold, the grasping is considered as failed.

To determine whether the grasp is successful, we implemented a dual-criteria validation approach. First, our algorithm analyzes the relative motion between the object and its supporting wires by calculating the differential displacement in consecutive time steps $(t-1, t)$. A successful grasp requires that this differential remain below a configurable threshold δ, expressed as $|z_{obj}(t) - z_{obj}(t-1)) - \frac{1}{4}\sum_{i=1}^{4}(z_{wire_i}(t) - z_{wire_i}(t-1))| < \delta$. Simultaneously, the system monitors orientation stability using quaternion mathematics, where the angular deviation θ between the current and initial orientation must not exceed a predefined threshold θ_{max}. This is calculated by converting the quaternions to rotation matrices, deriving the relative rotation matrix $R_{relative} = R_{current}R_{initial}^{T}$, and extracting θ from its trace. These criteria ensure synchronous vertical movement with the lifting mechanism and the maintenance of proper spatial orientation throughout the elevation process, providing comprehensive and robust validation of successful grasping operations.

IV. Result

A. Grasping pose pipeline setup

To evaluate the effectiveness of the proposed grasp generation and validation algorithm, we applied the pipeline to two distinct 3D test objects of varying geometries. Figure 3 illustrates the visualizations of both objects along with their corresponding 2D bitmap projections viewed from the Z-axis. The experimental parameters, such as bitmap resolution, scaling factor, dilation iterations, and grasping constraints, are summarized in Table I. These parameter values were empirically chosen to balance computational efficiency with grasp quality and spatial coverage.

B. Contour Extraction and Point Sampling

The contour extraction and morphological dilation process was successful in expanding the silhouettes of the projected 3D models. Figure 4 shows the resulting grasp candidate points along the expanded boundaries. A total of $n_{\text{target}} + 1$ points were obtained after down sampling to ensure even distribution. Each candidate was classified into one of three categories: concave, flat, or convex, based on curvature analysis. As expected, points classified as convex—marked in green—were excluded from grasp consideration due to the risk of wire slippage. However, due to the aggressive dilation iterations, some regions near original corners became rounded, allowing a few marginal convex points to appear near previously sharp edges. The quiver plot indicates the bending direction of the hook at each selected point, with vectors oriented perpendicularly toward the object's interior to ensure stable grasping. Subsequently, all valid 4-point combinations that satisfy the algorithmic constraints were systematically identified and appended to the set of solutions. These computed combinations were then used as input parameters for the physics simulation, where their grasping performance was evaluated under realistic loading conditions.

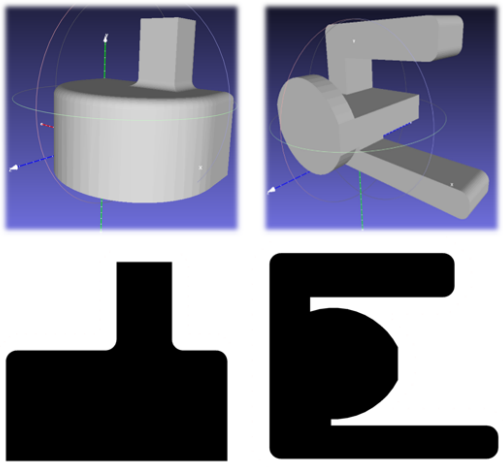

Fig. 3. Test object 1 and 2 and their Bitmap under birdview from Z-axis

TABLE I
EXPERIMENT PARAMETERS SETUP

Parameter Name	Value
Size of Bitmap (W, H)	$(2500, 2500)$
Bitmap scaling factor (s)	100
Number of target points before reduction (n_{target})	80
Number of iterations (n_{iter})	150
Minimum point selection interval (n_{interval})	2
Threshold angle for defining convex corner (θ_{cvx})	10°
Distance threshold factor (d)	0.03

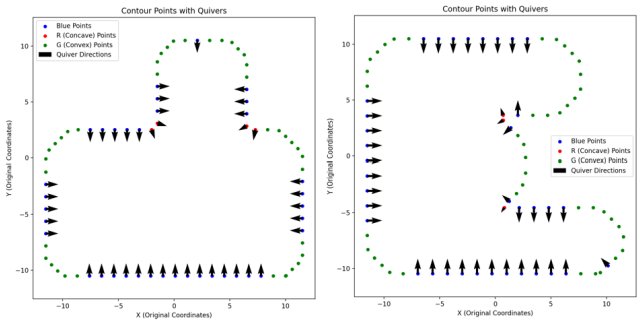

Fig. 4. Candidate grasp points after dilation and sampling. Green: convex (ignored), Red: concave, Blue: flat. Arrows indicate hook bending direction.

C. Physics Simulation Setup

For the simulation validation, we implemented a physics-based environment in NVIDIA Isaac Sim to assess the efficacy of the generated grasp configurations. Each test scenario comprised the target object and four articulated wire hooks positioned according to the coordinates and orientations determined by our algorithm. Figure 5 illustrates representative grasping configurations for both test objects, with subfigures 5(a) through 5(c) depicting three distinct grasping combinations for test part 1, and subfigures 5(d) through 5(f) showing equivalent combinations for test part 2.

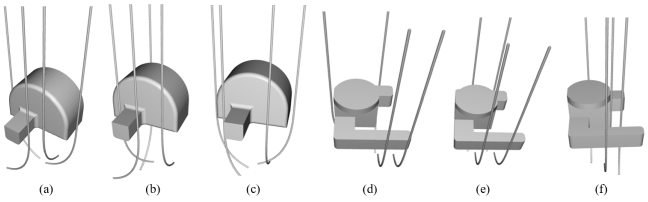

Fig. 5. Examples of representative grasping configurations for both test objects.

The simulation parameters of physics were carefully calibrated to ensure realistic behavior while maintaining computational efficiency, as detailed in Table II. In particular, we employed convex decomposition for mesh collision detection to balance accuracy with performance. Each hook was connected to its base via a prismatic joint constrained to move exclusively along the Z-axis, with an actuator upper limit of 0.8 m and a target velocity of 0.1 m/s. The substantial stiffness and damping coefficients (10,000 units each) ensured minimal joint deflection under load, effectively mimicking rigid mechanical linkages.

TABLE II
PHYSICS SIMULATION SETUP

Parameter Name	Value
Mesh collider type	Convex Decomposition
Joint type	Prismatic Joint
Joint direction	$Z - axis$
Actuator Upper limit	$0.8m$
Linear driver target velocity	0.1m/s
Minimum point selection interval (n_{interval})	2
Linear drive stiffness	10000
Linear drive damping	10000
fall threshold	$0.005m$
tilt threshold	10°
Simulation duration for each combination	$10s$

Table III summarizes the comprehensive simulation results for both test geometries. For part 1, our algorithm identified 41 valid candidate points, yielding 274 potential four-point grasping combinations. Among these configurations, 249 successfully maintained both position and orientation stability throughout the lifting process, resulting in a success rate of 91%. Test part 2, with 39 valid candidate points, generated 161 potential grasping combinations, of which 143 demonstrated successful performance, corresponding to a success rate 89%.

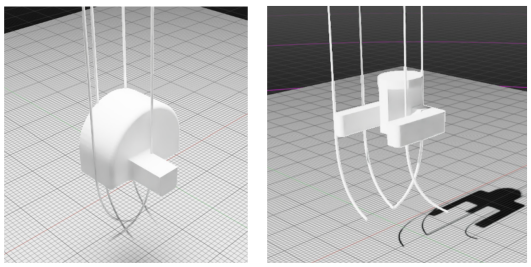

Fig. 6. Successful grasping cases for both parts in the ISAAC environment

TABLE III
REAL-TIME SIMULATION RESULT

Parameter Name	Test part 1	Test part 2
number of valid candidate points	41	39
number of valid combinations	274	161
number of cases falling	25	18
number of cases tilting	0	0
number of success combinations	249	143
Successful rate	91%	89%

V. CONCLUSION AND DISCUSSION

This project presents a novel algorithm for automated point generation specifically designed for wire grippers in the manufacturing of binder-jet metal additives. Our approach integrates 2D projection techniques, morphological operations, curvature analysis, and physics-based validation to reliably identify successful grasping configurations for part extraction during the depowdering phase. The direction-aware placement of the wire hooks ensures proper alignment with the surface of the parts, allowing safe lifting while maintaining structural integrity.

The physics-based simulation provides critical validation of generated configurations under realistic loading conditions, significantly enhancing the method's practical reliability. Experimental results demonstrate robust performance, with success rates of 91% and 89% for our test geometries. All observed failure modes involved excessive vertical displacement rather than orientation instability, suggesting the method effectively maintains grip alignment. However, these results should be interpreted with caution due to the limited sample size of test objects. Future work should include more extensive testing with geometrically complex parts to fully validate the method's generalizability.

Despite the promising results, several limitations warrant consideration. Firstly, the algorithm prioritizes geometric features without considering material properties such as density distribution, mechanical strength, or surface friction, which could significantly impact grasp performance in real-world scenarios. For parts with non-uniform density or fragile regions, additional constraints would be necessary to ensure safe handling. Secondly, the simulation environment, while sophisticated, does not fully replicate the challenges of extracting parts from a powder bed, including potential suction effects, powder adhesion, or neighboring part interference. These factors could introduce additional constraints on viable

grasp configurations that are not currently captured in our validation process.

It is important to note that the current implementation merely filters all combinations that meet the constraints specified in the algorithm without identifying the optimal grasping configuration. This approach, while effective for generating viable solutions, does not necessarily yield the most efficient or stable grasp for a given part geometry. Future iterations should incorporate a cost function or value function to quantitatively evaluate and rank grasp combinations, enabling the identification of truly optimal grasping strategies.

VI. Future Works

Several promising directions for future research emerge from this work. First, further validation using more complex geometries with intricate features and undercuts is necessary to comprehensively assess the algorithm's limitations and robustness.

Secondly, the experimental setup and input variables might need to be adjusted when dealing with different object geometries and scales. Future research should focus on developing adaptive parameter selection mechanisms that can automatically configure optimal settings based on part characteristics, ensuring robust performance across diverse geometries without manual tuning. This would significantly enhance the versatility and practical applicability of the algorithm.

In addition, integrating machine learning approaches could improve the selection of grasp points by learning from successful and failed grasp attempts across various geometries of parts. A neural network trained in physics simulation outcomes could potentially predict grasp success probability without requiring exhaustive simulation of all candidate configurations, thereby streamlining the planning process.

Acknowledgment

The author gratefully acknowledges the assistance of all members of CERLAB, and the invaluable guidance of Dr. Kenji Shimada.

References

[1] Wei Gao, Yunbo Zhang, Devarajan Ramanujan, Karthik Ramani, Yong Chen, Christopher B. Williams, Charlie C.L. Wang, Yung C. Shin, Song Zhang, and Pablo D. Zavattieri. The status, challenges, and future of additive manufacturing in engineering. *Computer-Aided Design*, 69:65–89, 2015.

[2] Wenchao Du, Wenhua Yu, David M. France, and Dileep Singh. Depowdering of an additively manufactured heat exchanger with narrow and turning channels. *Additive Manufacturing Letters*, 9:100202, 2024.

[3] Zhenwei Liu, Junyi Geng, Xikai Dai, Tomasz Swierzewski, and Kenji Shimada. Robotic depowdering for additive manufacturing via pose tracking. *IEEE Robotics and Automation Letters*, 7(4):10770–10777, October 2022.

[4] Douglas Morrison, Peter Corke, and Jürgen Leitner. Closing the loop for robotic grasping: A real-time, generative grasp synthesis approach, 2018.

[5] Abdulhamid Mathkur, Yanen Huang, and Kenji Shimada. Novel wire gripper for robotics picking of small green parts from powder bed of binder jet metal additive manufacturing. *IEEE Access*, pages 1–1, 2025.

[6] J. Cormack, M. Fotouhi, G. B. Adams, and A. G. Pipe. Automated extraction of 3d printed parts from unfused pa12 powder using a one-shot 3d printed compliant gripper. *IEEE Robotics and Automation Letters*, 6(4):8655–8662, 2021.

[7] R. Chen, R. Song, Z. Zhang, L. Bai, F. Liu, P. Jiang, D. Sindersberger, G. J. Monkman, and J. Guo. Bio-inspired shape-adaptive soft robotic grippers augmented with electroadhesion functionality. *Soft Robotics*, 6(6):701–712, 2019.

[8] A. M. Razali, A. Abdul Aziz, and S. Ahmad. Optimum design of multifunction robotic arm grippers for varying shapes of green products. *Journal of Manufacturing Processes*, 23:167–174, 2016.

[9] H. S. Lee, S. W. Park, and J. Kim. Powder spreading and densification process in binder jetting additive manufacturing. *International Journal of Advanced Manufacturing Technology*, 123(1):95–108, 2022.

[10] Hamidreza Kasaei and Mohammadreza Kasaei. Mvgrasp: Real-time multi-view 3d object grasping in highly cluttered environments. *Robotics and Autonomous Systems*, 160:104313, 2023.